Proceedings of the ASME 2009 7th International Conference on Nanochannels, Microchannels and Minichannels
ICNMM2009
June 22-24, 2009, Pohang, South Korea

ICNMM2009-82150

KEYNOTE PAPER

LIQUID FILM THICKNESS IN MICRO CHANNEL SLUG FLOW

Naoki Shikazono and Youngbae Han
Department of Mechanical Engineering,
The University of Tokyo,
Hongo 7-3-1, Bunkyo-ku, Tokyo, Japan
e-mail: shika@feslab.t.u-tokyo.ac.jp

ABSTRACT

Slug flow is the representative flow regime of two-phase flow in micro channels. It is well known that the thin liquid film formed around the confined vapor bubble plays an important role in micro channel heat transfer. In the present study, experiments are carried out to clarify the effects of parameters that affect the formation of the thin liquid film in micro channel slug flow. Laser focus displacement meter is used to measure the thickness of the thin liquid film. Air, ethanol, water and FC-40 are used as working fluids. Circular tubes with five different diameters, D = 0.3, 0.5, 0.7, 1.0, 1.3 mm, and square channels with two different sizes, 0.3 x 0.3 and 0.5 x 0.5 mm, are used. It is confirmed that the liquid film thickness is determined only by capillary number at small capillary numbers. However, the effect of inertial force and flow acceleration cannot be neglected as capillary number increases. The effect of cross sectional shape is also investigated. Experimental correlation for the adiabatic liquid film thickness in circular tubes based on capillary number, Reynolds number and Weber number is proposed. When viscous boundary layer is thin, liquid film thickness is limited by the viscous boundary layer thickness. Thus, in order to develop precise flow boiling models in micro tubes, it is important to consider the effects of inertial force and boundary layer thickness on the liquid film thickness.

1. INTRODUCTION

Thin liquid film formed around the confined vapor bubble in micro channels plays an important role in micro heat exchangers and micro reactors, since local heat and mass transfer is effectively enhanced at the thin liquid film region. However, flow characteristics in micro channels are not fully understood, and thus two-phase flow system design still remains as a difficult task. It is reported that the thickness of the liquid film is one of the important parameters for the prediction of flow boiling heat transfer in micro tubes, e.g., Thome et al. (2004), Dupont et al. (2004) and Kenning et al. (2006). In their models, liquid film thickness is introduced as one of the most important parameters.

Many researches on the liquid film thickness in macro channel slug flows have been conducted both experimentally and theoretically. Taylor (1961) experimentally obtained the mean liquid film thickness remaining on the wall by measuring the difference of the bubble velocity and the mean velocity. Highly viscous fluids, i.e., glycerin, syrup-water mixture and lubricating oil, were used so that wide capillary number range could be covered. It is reported that the liquid film thickness increases with capillary number and reaches a certain fraction of the tube diameter. Bretherton (1961) suggested an analytical theory on the bubble profile and axial pressure drop across the bubble with the lubrication equations. Assuming small capillary number, it is shown that the dimensionless liquid film thickness can be scaled with $Ca^{2/3}$. Moriyama & Inoue (1996) obtained the liquid film thickness formed by a vapor bubble expansion in a narrow gap by measuring the temperature change of the channel wall which was initially superheated. In their experiment, it was assumed that whole liquid film on the wall evaporates, and the heat is consumed by the evaporation of the liquid film. Their experimental data was correlated in terms of capillary number and Bond number based on the interface acceleration. Heil (2001) investigated the effect of inertial force on the liquid film thickness numerically. It is shown that the liquid film thickness and the pressure gradient are dependent on the Reynolds number. Aussillous & Quere (2000) measured the liquid film thickness using fluids of relatively low surface tension. It was found that the liquid film thickness deviates from the Taylor's data at relatively high capillary numbers. Visco-inertia regime, where the effect of inertial force on the liquid film thickness becomes significant, was demonstrated. Kreutzer et al. (2005) investigated the liquid film thickness and the pressure drop in a micro tube both numerically and experimentally. Predicted liquid film thickness showed almost the same trend with that reported by Heil (2001). Utaka et al. (2007) measured the liquid film thickness formed by a vapor bubble in a narrow gap

mini-channel with laser extinction method. It was concluded that the boiling phenomena were determined by two kinds of characteristic periods, i.e., the micro-layer dominant and the liquid saturated periods.

Although many experiments have been carried out to measure the liquid film thickness, quantitative data of local and instantaneous liquid film thicknesses are still limited. To develop a precise heat transfer model in micro tubes, it is crucial to predict the liquid film thickness around the confined bubble. In the present study, local and instantaneous liquid film thicknesses are measured directly with laser focus displacement meter. Series of experiments is conducted to investigate the effects of parameters, i.e., viscous, surface tension and inertial forces, cross sectional shapes, acceleration and wall superheat, on the formation of liquid film in micro channel slug flow.

NOMENCLATURE

Symbol	Description	Unit
Ca	Capillary number	-
D	Tube diameter	m
G	Mass flow rate	kg/m^{2}s
L	Distance from the measuring point	m
n	Refractive index	-
Re	Reynolds number	-
U	Bubble Velocity	m/s
We	Weber number	-

Greek Symbols

δ	Liquid film thickness	m
μ	Viscosity	Pa·s
ν	Kinematic viscosity	m^2/s
ρ	Density	kg/m^3
σ	Surface tension	N/m

Subscripts

0	Initial
sat	Saturated
super	Superheat
wall	Tube wall

2. EXPERIMENTAL SETUP AND PROCEDURES

2.1 Liquid film thickness experiment without phase change

Figure 1 shows the schematic of the experimental setup for measuring the adiabatic liquid film thickness. Refer to Han & Shikazono (2008, 2009a, 2009b) for details. One side of Pyrex glass tube is connected to the syringe. An actuator motor (EZHC6A-101, Oriental motor) was used to move the liquid inside the test section. The velocity of the actuator is varied from 0 to 0.6 m/s. Syringes with several cross sectional areas are used to control the liquid velocity in the test section. Thus, the range of liquid velocity in the present experiment is varied from 0 to 7 m/s. Velocity and acceleration is controlled by the actuator motor. The velocity of the vapor bubble is measured from the images captured by the high-speed camera (Phantom 7.1). The images are taken at several frame rates according to the bubble velocity. For the maximum bubble velocity, frame rate is 10000 frames per second with a shutter time of 10 μs.

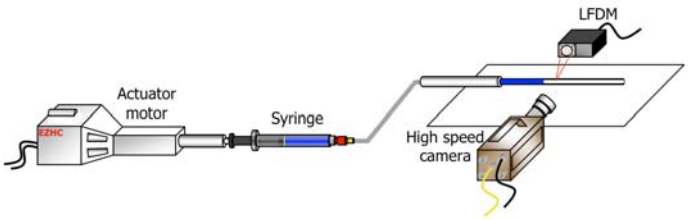

Fig. 1 Schematic diagram of the experimental setup

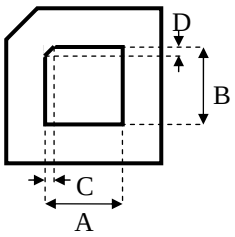

Fig. 2 Cross section of the square channels

Table 1 Dimensions of the circular tubes

I.D. (mm)	O.D. (mm)	Length (mm)
0.487	0.6	250
0.715	1.0	250
0.995	1.6	250
1.305	1.6	250

Table 2 Dimensions of the square channels

	A (mm)	B (mm)	C (mm)	D (mm)
0.3 × 0.3 mm	0.294	0.283	0.019	0.014
0.5 × 0.5 mm	0.559	0.571	0.044	0.041

Laser focus displacement meter (LT9010M, Keyence) is used to measure the thickness of the liquid film. The displacement of the target surface can be determined by the objective lens activated by the tuning fork. Takamasa & Kobayashi (2000) and Hazuku et al. (2005) have used laser focus displacement meter for measuring the liquid film thickness. It is reported that laser focus displacement meter can measure the liquid film thickness very accurately within 1% error. The intensity of the reflected light becomes highest in the light-receiving element when the focus is obtained on the target surface. The resolution of the present laser focus displacement meter is 0.01 μm, the laser spot diameter is 2 μm and the response time is 640 μs. Thus, it is possible to measure instantaneous and local liquid film thickness. Measured liquid film thickness is transformed to DC voltage signal in the range of ±10V. Output signal was sent to PC through GPIB interface and recorded with LabVIEW.

Tube diameter was measured with a microscope and the averaged value of the inlet and outlet inner diameters was used. Tables 1 and 2 show the dimensions of the circular tubes and square channels used in the present study. One corner of the square channel is modified to measure the liquid film thickness at the channel corner. The differences of inlet and outlet inner diameters are less than 1% for all tubes. For circular tubes, cover glass and glycerol were used to remove the focus scattering caused by the outer wall curvature. Figure 3 shows

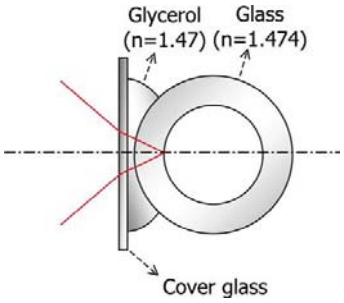

Fig. 3 Correction for the outer wall curvature.

Table 3 Properties of the working fluids at 25℃ and 1 atm.

	Water	Ethanol	FC-40
ρ (kg/m^3)	997	785	1849
μ (mPa·s)	889	1088	3260
σ (mN/m)	70.0	22.3	16.0
n	1.33	1.36	1.29

the schematic of the micro tube with cover glass and glycerol. As the laser beam passes through the tube wall, focus is scattered within a certain range due to the difference of curvatures between axial and azimuthal directions. Refractive index of glycerol (n = 1.47) is almost the same with that of the Pyrex glass (n = 1.474), so the refraction of laser between glycerol and Pyrex glass can be neglected. Refractive indices of ethanol, water are 1.36 and 1.33 under the condition of 1 atm and 25 ℃. It is difficult to detect the inner wall/liquid interface and the liquid/gas interface simultaneously, because the difference of the refractive indices of the wall and the liquid is small. Therefore, the distance from the cover glass to the dry inner wall is initially measured without flowing the liquid. Then, the thickness with liquid film is measured. The liquid film thickness is calculated from the difference of these two values. The effect of the inner wall curvature is corrected by the equation suggested by Takamasa & Kobayashi (2000). The inner wall curvature effect on liquid film thickness is not large when the liquid film is thin. The scattering depth due to this inner wall curvature is less than 2% of the liquid film thickness in the present experiments.

To investigate the effects properties on the liquid film thickness, three working fluids, water, ethanol and FC-40, were used. All adiabatic experiments were conducted under the condition of room temperature and 1 atm. Table 3 shows the properties of three liquids at 25℃ and 1 atm. Figure 4 shows the Reynolds number and the capillary number for the present experimental conditions. Reynolds number of ethanol is about 6 times larger than that of FC-40, and Reynolds number of water is about 6 times larger than that of ethanol at the same capillary number.

Figure 5 shows a typical measurement example. There is no signal before the air-liquid interface reaches the measuring position. After air-liquid interface passes by the measuring position, liquid film is formed on the wall and signal is obtained. In Fig. 5, liquid film thickness shows rapid initial decrease. This initial decrease corresponds to the transition from the bubble nose to the flat film region. In the present study, liquid film thickness measured from the tube side is collected as the experimental data.

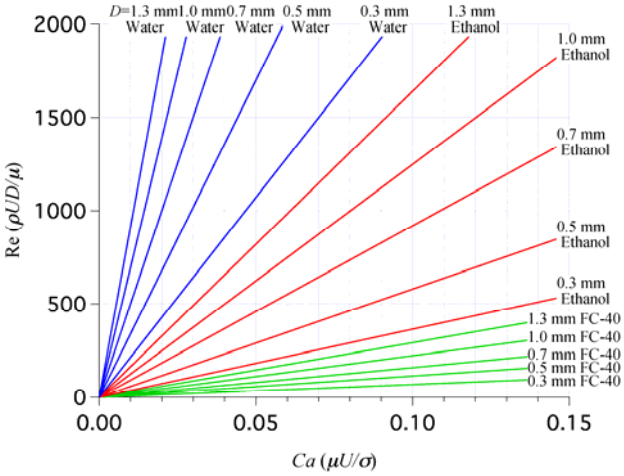

Fig. 4 Reynolds number against capillary number for the present experiment.

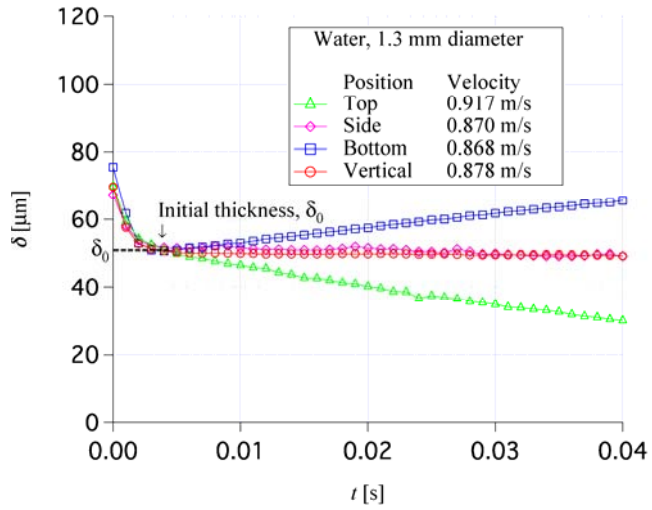

Fig. 5 Measured liquid film thickness against time

2.2 Boiling experiment

Under heated or flow boiling conditions, effects of wall superheat and acceleration must be considered. For the boiling experiment, only inner diameter 0.5 mm tube and ethanol are used. Figure 6 shows the schematic diagram for the boiling experiment. Working fluid is degassed by a degasser and pumped at a uniform flow rate with a plunge pump. Ethanol is heated to the saturated temperature and small vapor bubble is generated periodically in the preheater. Generated vapor bubble from the preheater flows into the test section and expands due to wall superheat. Test tube is coated by ITO, which is a transparent conductive layer for Joule heating. ITO film is connected to the DC power supply. Outer wall temperatures are measured by K-type thermocouples calibrated within ±0.1°C error. Inner wall temperatures are calculated from the 1D heat conduction equation. Figure 7 shows the heating section and the liquid film measuring point. Gas/liquid interface velocity and the liquid film thickness are measured by the high-speed camera and the laser focus displacement meter in the same way as the adiabatic experiment.

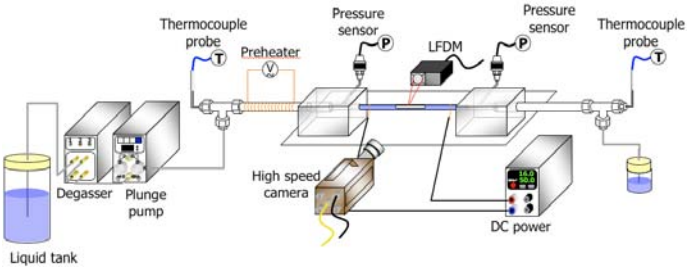

Fig. 6 Schematic diagram of the boiling experiment setup.

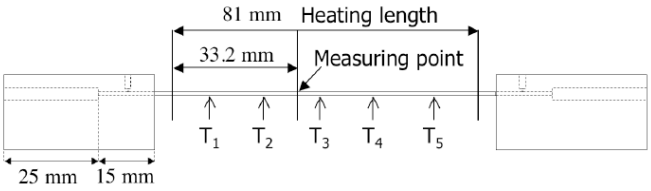

Fig. 7 Measuring points and heating length.

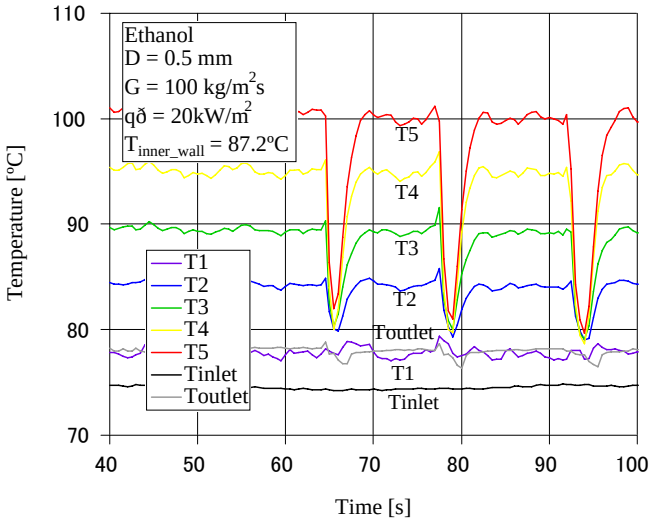

Fig. 8 Inner wall temperature against time.

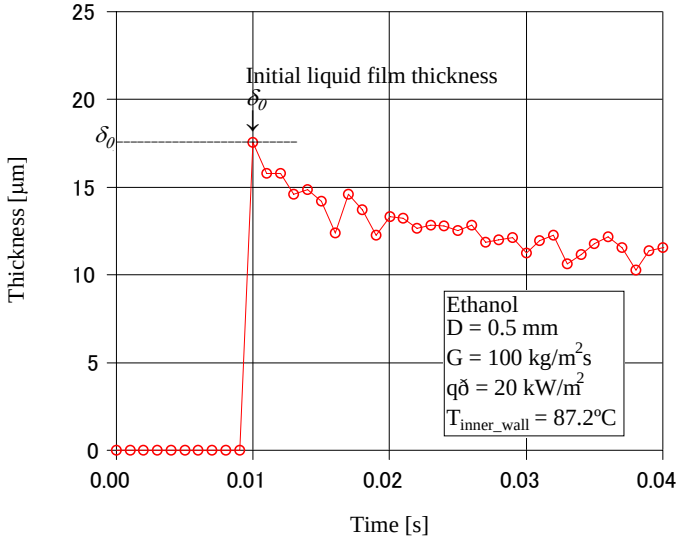

Fig. 9 Liquid film thickness against time.

Figures 8 and 9 show typical boiling experiment data. Experimental condition is ethanol, D = 0.5 mm, G = 100 kg/m^{2}s, q'' = 20 kW/m^2, and the inner wall temperature at the measuring point was T_{inner_wall} = 87.2°C. In Fig. 8, vapor bubble generated in the preheater flows into the test tube periodically and phase change takes place in the test section. In the present experiment, vapor bubble is not generated until wall superheat becomes larger than 35°C. Therefore, liquid flow in the test section becomes superheated. Figure 9 shows the change of liquid film thickness with time when the vapor bubble expands. When the measuring point is filled with liquid, there is no signal obtained from the laser focus displacement meter. After bubble nose passes by the measuring point, liquid film is formed on the tube wall and the signal for the liquid film thickness can be obtained. Bubble velocity and acceleration are calculated from the images captured by the high-speed camera. In Fig. 9, unlike the adiabatic condition, liquid film thickness does not become constant but decreases monotonously due to evaporation. Since no plateau can be observed for the liquid film thickness in Fig. 9, initial value is taken as the liquid film thickness δ_0.

3. RESULTS AND DISCUSSION

3.1 Adiabatic liquid film thickness in circular tubes

Figure 10 shows the dimensionless liquid film thickness for FC-40, ethanol and water for the adiabatic experiments. The solid line in Fig. 10 is an empirical fitting curve of Taylor's experimental data proposed by Aussillous & Quere (2000).

$$\frac{\delta}{D} = \frac{0.67Ca^{2/3}}{1+3.35Ca^{2/3}} \qquad (1)$$

Equation (1) is called Taylor's law. The working fluids in Taylor's experiments were highly viscous such as glycerol and sugar-water syrup. Therefore, Reynolds number in Taylor's experiment was small and the inertial force is negligible. At low Ca, dimensionless liquid film thicknesses for three liquids become nearly identical with the Taylor's law. Thus, the inertial force can be neglected in this region, and the dimensionless liquid film thickness is determined only by the capillary number. At large Ca, all FC-40 data are smaller than the Taylor's law. On the other hand, ethanol and water data become much larger than the Taylor's law as tube diameter increases. It is obvious that inertial force strongly affects liquid film thickness at relatively large Reynolds numbers. At Re > 2000, liquid film thickness does not increase but remains nearly constant with some scattering. In Fig. 10 (c), points of Re≒2000 in each tube are indicated. Thus, this trend is considered to be the flow transition from laminar to turbulent of the liquid phase.

Figure 11 shows the measured dimensionless liquid film thickness with the numerical simulation results obtained by Kreutzer et al. (2005). Dimensionless liquid film thickness at a particular capillary number is obtained from the fitting curve of the experimental data. Dimensionless liquid film thicknesses are nearly constant against Reynolds number at small capillary numbers. Therefore, at small capillary numbers, inertial force can be neglected and liquid film thickness is determined only by capillary number. As capillary number increases, the dimensionless liquid film thickness is dependent on Reynolds number and takes a

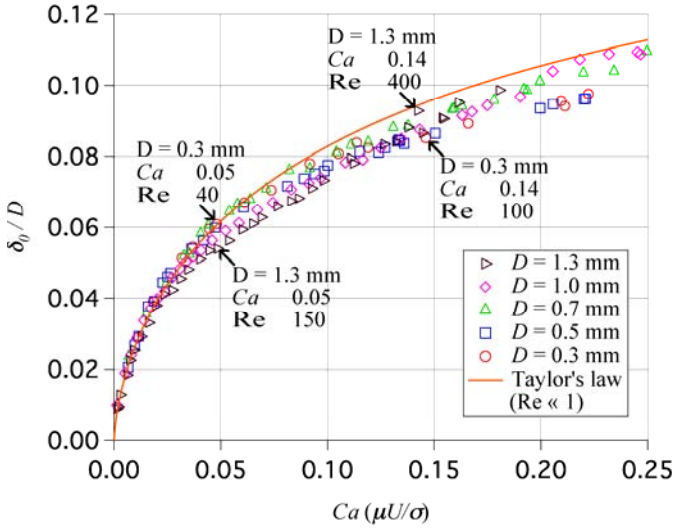

(a) FC-40

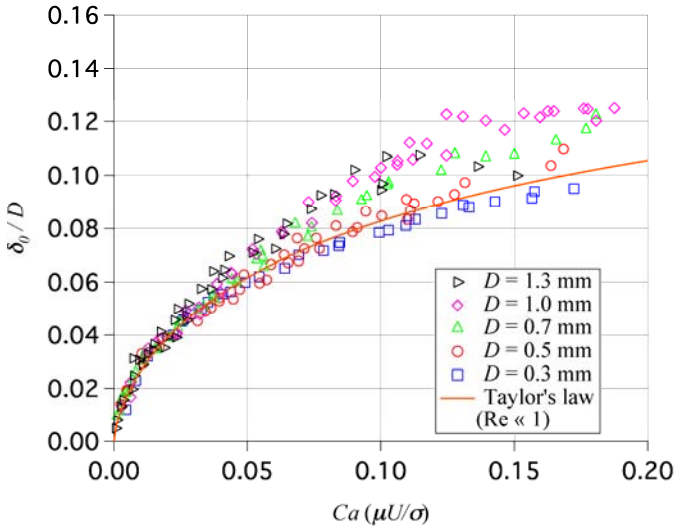

(b) Ethanol

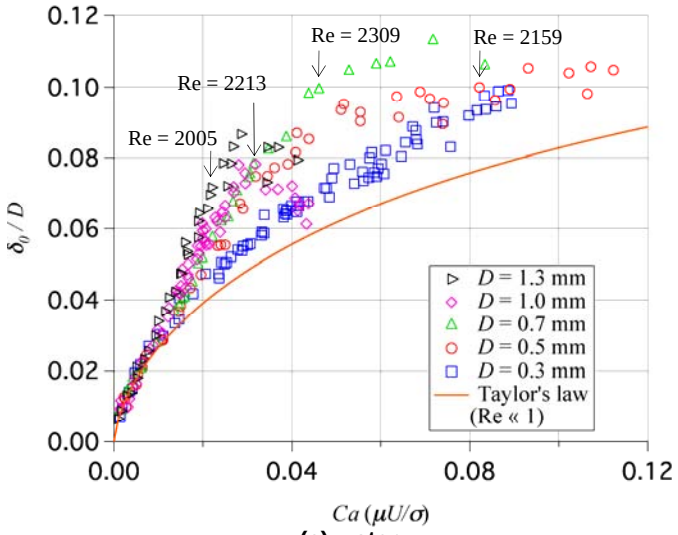

(c) water

Fig. 10 Dimensionless initial liquid film thickness.

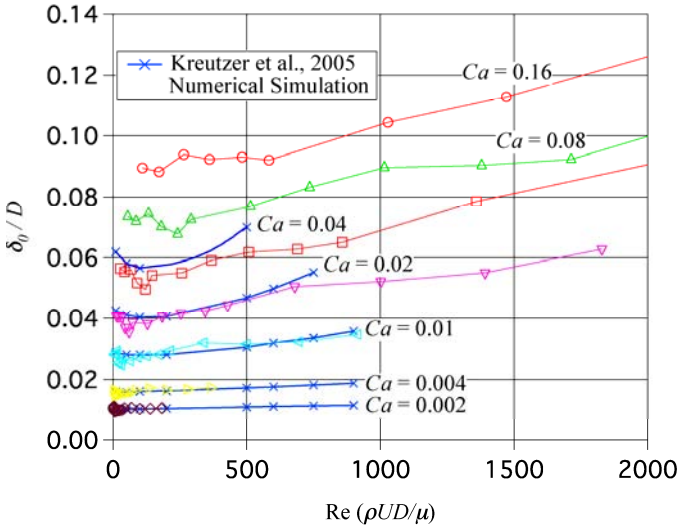

Fig. 11 Reynolds number dependence of the dimensionless liquid film thickness.

minimum value against Reynolds number. This effect of inertial force on the liquid film thickness is also observed in the numerical simulation results of Kreutzer et al. (2005) as shown in Fig. 11.

Aussillous & Quere (2000) replaced the curvature of the bubble nose $\kappa=1/(D/2)$ with $\kappa=1/\{(D/2)-\delta_0\}$ in the Bretherton's theoretical analysis (1961), and obtained the following relation:

$$\frac{\delta_0}{D/2} \approx \frac{Ca^{2/3}}{1+Ca^{2/3}}. \qquad (2)$$

In Eq. (2), dimensionless liquid film thickness asymptotes to a finite value due to the term $Ca^{2/3}$ in the denominator. Based on Eq. (2), Taylor's experimental data was fitted as Eq. (1). If the effect of inertial force is taken into account, the momentum balance and the curvature matching between the bubble nose and the transition region should be expressed as follows:

$$\frac{\mu U}{\delta_0^2} \approx \frac{1}{\lambda}\left\{\frac{\sigma}{(D/2)+\delta_0}\right\} - \frac{1}{\lambda}\rho U^2, \qquad (3)$$

$$\frac{\delta_0}{\lambda^2} \approx \frac{\sigma}{(D/2-\delta_0)}. \qquad (4)$$

We can deduce the relation of δ_0/D from Eqs. (3) and (4) as:

$$\frac{\delta_0}{D/2} \approx \frac{Ca^{2/3}}{Ca^{2/3}+(1-We')^{2/3}}, \qquad (5)$$

where Weber number is defined as We' = $\rho U^2((D/2)-\delta_0)/\sigma$. Equation (5) is always larger than Eq. (2) because the sign in front of Weber number is negative. Therefore, Eq. (5) can express the increase of the liquid film thickness with Weber number. On the other hand, Heil (2001) reported that inertial force makes the bubble nose slender and increases the bubble nose curvature. It is also reported in Edvinsson & Irandoust (1996) and Kreutzer et al. (2005) that the curvature of bubble nose increases with Reynolds number and capillary number. This implies that curvature term $\kappa = 1/\{(D/2)-\delta_0\}$ in the momentum equation should become larger with Reynolds number and capillary number. We assume that this effect of curvature change can be expressed by adding a function of

Reynolds number and capillary number to $\kappa = 1/\{(D/2)-\delta_0\}$ term as:

$$\kappa = \frac{1+f(\mathrm{Re},Ca)}{(D/2)-\delta_0}. \quad (6)$$

Substituting Eq. (6) into Eqs. (3) and (4), and assuming that Re, Ca and We terms are effectively small, we obtain:

$$\frac{\delta_0}{D/2} \approx \frac{Ca^{2/3}}{Ca^{2/3}+1+f(\mathrm{Re},Ca)-g(We)}. \quad (7)$$

Finally, the experimental data is correlated by least linear square fitting in the form as:

$$\frac{\delta_0}{D} = \frac{0.67Ca^{2/3}}{1+3.13Ca^{2/3}+0.504Ca^{0.672}\,\mathrm{Re}^{0.589}-0.352We^{0.629}} \quad (\mathrm{Re}\le 2000), \quad (8)$$

where Ca = $\mu U/\sigma$, Re = $\rho UD/\mu$ and We = $\rho U^2 D/\sigma$. Equation (8) should follow Bretherton's theory as capillary number approaches to zero. So the coefficient in the numerator is taken as 0.670.

When Reynolds number becomes larger than approximately 2000, liquid film thickness remains nearly constant as shown in Fig. 10 (c). Since *Ca*/Re takes a constant value for a given tube diameter and working fluid as shown in Fig. 4, liquid film thickness for Re>2000 is given as:

$$\frac{\delta_0}{D} = \frac{106\left(\frac{Ca}{\mathrm{Re}}\right)^{2/3}}{1+497\left(\frac{Ca}{\mathrm{Re}}\right)^{2/3}+7330\left(\frac{Ca}{\mathrm{Re}}\right)^{0.672}-5000\left(\frac{Ca}{\mathrm{Re}}\right)^{0.629}} \quad (\mathrm{Re}>2000), \quad (9)$$

Figures 12 and 13 show the comparison between the experimental data and the predictions of Eqs. (8) and (9). The present correlation can predict δ_0 within the range of $\pm$15% accuracy.

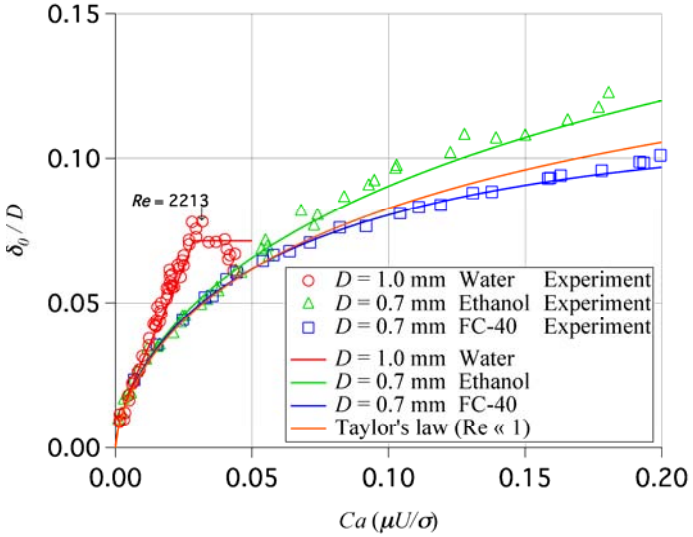

Fig. 12 Predicted liquid film thickness.

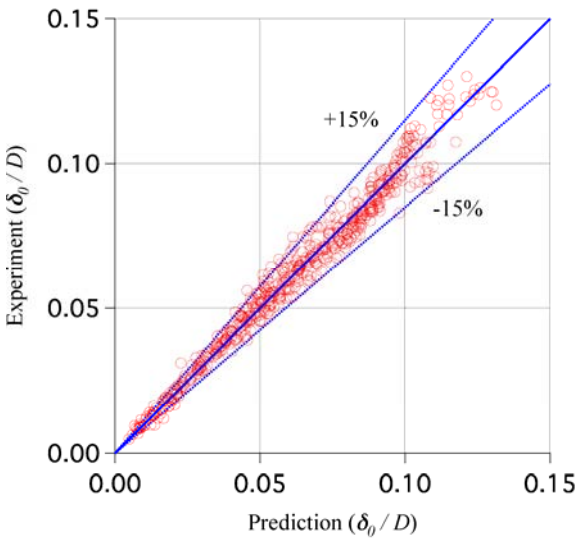

Fig. 13 Comparison between predicted and measured liquid film thicknesses.

3.2 Liquid film thickness with acceleration

Figures 14 and 15 show the dimensionless liquid film thickness under constant acceleration. For fixed measurement distance *L*, acceleration is larger for larger capillary numbers. Liquid film thickness is identical with the zero acceleration data at small capillary numbers. However, as capillary number increases, liquid film thickness becomes smaller than the zero acceleration case. For *D* = 0.7 and 1.0 mm tubes, liquid film thicknesses show slight decrease. It is considered that viscous boundary layer thickness affects the liquid film thickness. When the bubble is accelerated, viscous boundary layer grows due to velocity change. It is reported that the liquid film thickness is limited by the viscous boundary layer when viscous boundary layer thickness is very thin (Moriyama & Inoue, 1996; Aussillous & Quere, 2000). Figure 16 shows the dimensionless liquid film thickness against dimensionless viscous boundary layer thickness. In Fig. 16, it is shown that experimental values approach to an asymptotic line. This line corresponds to the limitation of the liquid film thickness caused by the viscous boundary layer. The slopes of the asymptotic lines are different for ethanol and water. The reason for this difference is not clear and further investigation is required.

3.3 Liquid film thickness in square channels

Figure 17 shows the dimensionless liquid film thickness in micro square channels. In Fig. 17, hydraulic diameter D_h is used for normalizing the liquid film thickness. Liquid film thickness δ_0 at channel center is almost zero for *Ca* < 0.03. However, δ_0 at channel corner increases from *Ca* = 0. It is found that the effect of inertial force becomes more distinct at the channel corner than at the channel center. The dependence of δ_0 on inertial force is qualitatively the same with the circular tubes, but δ_0 for given capillary number is much thicker at the channel corner than that in the circular tubes. For Re > 2000, the liquid film thickness remains nearly constant also in square channels.

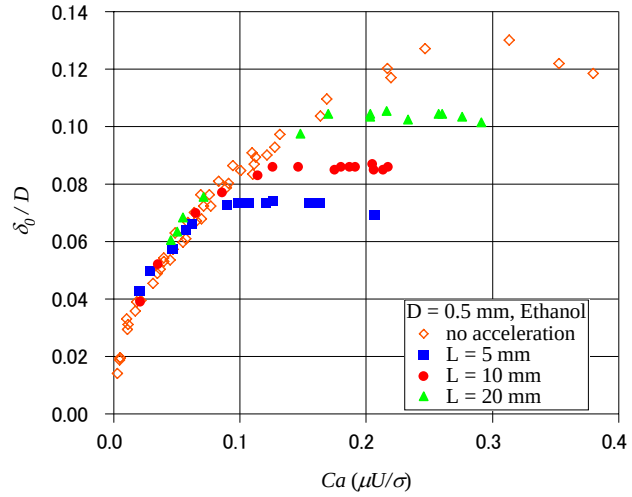

Fig. 14 Dimensionless liquid film thickness of ethanol at *L* = 5, 10 and 20 mm, *D* = 0.5 mm.

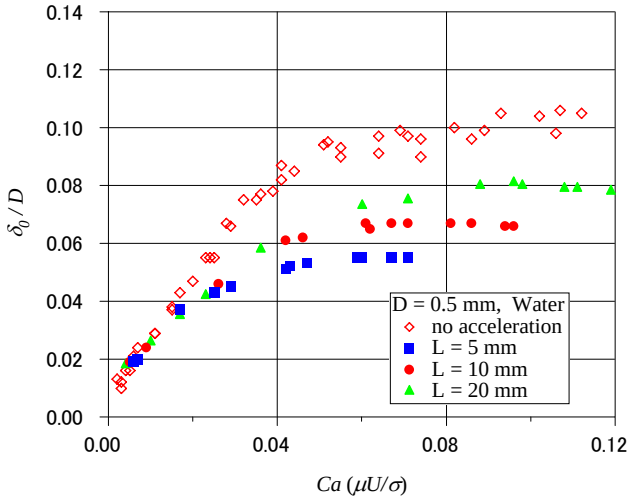

Fig. 15 Dimensionless liquid film thickness of water at *L* = 5, 10 and 20 mm, *D* = 0.5 mm

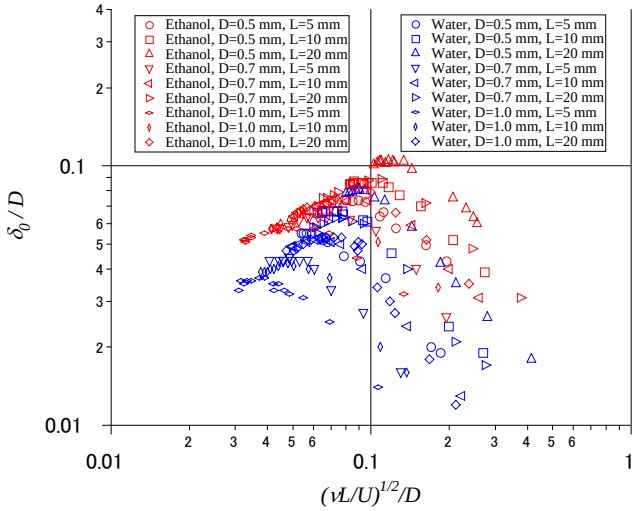

Fig. 16 Liquid film thickness against viscous boundary layer thickness.

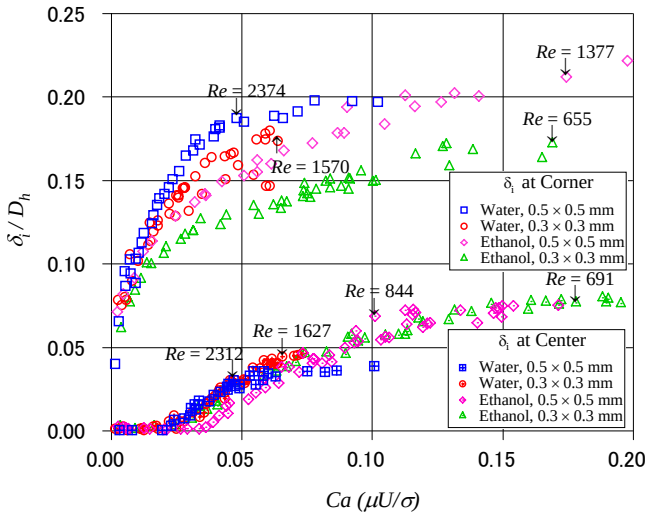

Fig. 17 Dimensionless liquid film thickness (δ_0/D_h) against capillary number ($Ca = \mu U/\sigma$) in square channels.

3.4 Liquid film thickness in boiling conditions

Figure 18 shows the dimensionless liquid film thickness against capillary number in boiling experiments. Solid line in Fig. 18 represents Eqs. (8) and (9). Properties at saturated temperature are used for the prediction. Square open symbols represent the data with wall superheat less than 5℃, and they follow the adiabatic prediction very well. Since the measuring point for this experiment is quite far from the nucleation site, viscous boundary layer is considered to be thick enough. However, as wall superheat increases, liquid film thickness becomes thinner than the adiabatic prediction. It is considered that the liquid viscosity near the wall decreases due to wall superheat. Saturation temperature can be used for the surface tension. However, viscosity should be treated carefully, since it is sensitive to temperature. Figure 19 shows the comparison between predicted liquid film thicknesses and the experimental data. Saturated temperature properties are used for the open square symbols and it is shown that the adiabatic prediction underestimates the experimental data. If wall temperature instead of saturation temperature is used for viscosity, agreement between prediction and experiment is excellent as shown by the open circles. Therefore, it is recommended to use wall temperature for viscosity when wall superheat is high.

4. CONCLUSIONS

The initial liquid film thicknesses in micro tubes and channels are measured directly by laser focus displacement meter. At small capillary numbers, the initial liquid film thickness is determined only by capillary number and the inertial effect is negligible. On the other hand, the effect of inertial force cannot be neglected as capillary number increases. At relatively large capillary number, liquid film thickness takes a minimum value against Reynolds numbers. If Reynolds number becomes larger than roughly 2000, liquid film thickness becomes nearly constant and shows some scattering. Empirical correlation for the dimensionless liquid film thickness in adiabatic circular tubes based on capillary number, Reynolds number and Weber number is proposed. The

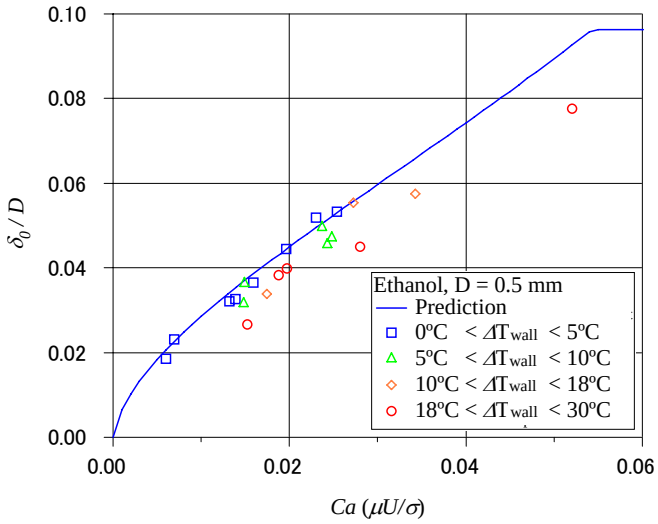

Fig. 18 Deviation from prediction value according to the wall superheat, ΔT_{wall}

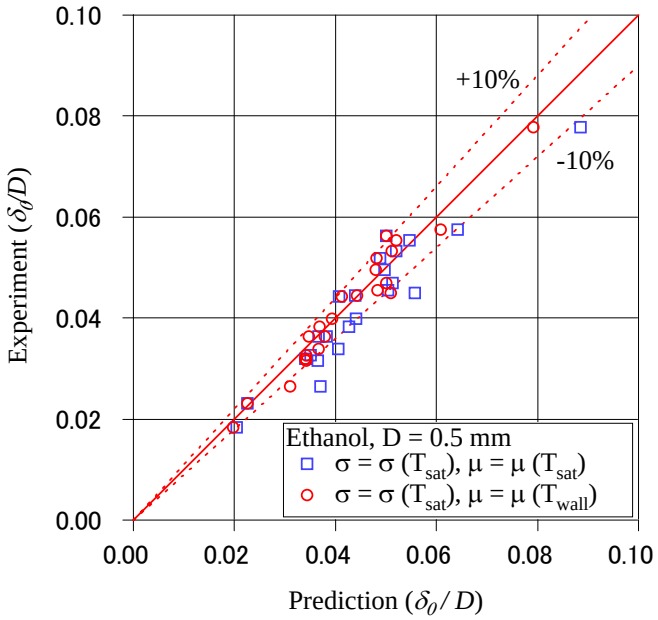

Fig. 19 Comparison of experimental and predicted data.

proposed correlation can predict the initial liquid film thickness within ±15% accuracy. When the bubble is accelerated, viscous boundary layer grows and this viscous boundary layer strongly affects the liquid film thickness. When the viscous boundary layer is thick, liquid film thickness can be determined by Eqs. (8) and (9). However, when the viscous boundary layer is thin, liquid film thickness is limited by the viscous boundary layer. Thus, in order to develop precise flow boiling models in micro tubes, it is necessary to consider the effects of inertial force as well as the viscous boundary layer development on the liquid film thickness.

ACKNOWLEDGEMENTS

We would like to thank Prof. Kasagi, Prof. Suzuki and Dr. Hasegawa for the fruitful discussions and suggestions. This work is supported through Grant in Aid for Scientific Research (No. 20560179) by MEXT, Japan..

REFERENCES

Aussillous, P., Quere, D., 2000, Quick deposition of a fluid on the wall of a tube, *Phys. of Fluids*, 12(10), 2367-2371.

Bretherton, F. P., 1961, The motion of long bubbles in tubes, *J. Fluid Mech.*, 10(2), 166-188.

Dupont, V., Thome, J. R., & Jacobi, A. M., 2004, Heat transfer model for evaporation in microchannels. Part I: comparison with the database, *Int. J. Heat Mass Transfer*, 47(14-16), 3387-3401.

Edvinsson, R. K. & Irandoust, S., 1996, Finite-element analysis of taylor flow, *AIChE J.*, 42(7), 1815-1823.

Han, Y. B. & Shikazono N., 2008, Measurement of the liquid film thickness in micro tube slug flow, *Proc. ECI Conf. on Heat Transfer and Fluid Flow in Microscale*, Paper 41.

Han, Y. B. & Shikazono N., 2009a, Measurement of the liquid film thickness in micro tube slug flow, *Int. J. Heat Fluid Flow*, to be published.

Han, Y. B. & Shikazono N., 2009b, Liquid film thickness in micro tube under flow boiling condition, to be presented at *7th Int. ASME Conf. on Nanochannels, Microchannels and Minichannels, ICNMM2009*.

Hazuku, T., Fukamachi, N., Takamasa, T., Hibiki, T. & Ishii, M., 2005, Measurement of liquid film in microchannels using a laser focus displacement meter, *Experiments in Fluids*, 38(6), 780-788.

Heil, M., 2001, Finite Reynolds number effects in the Bretherton problem, *Phys. of Fluids*, 13(9), 2517-2521.

Kenning, D. B. R., Wen, D. S., Das, K. S. & Wilson, S. K., 2006, Confined growth of a vapour bubble in a capillary tube at initially uniform superheat: Experiments and modeling, *Int. J. Heat Mass Transfer*, 49(23-24), 4653-4671.

Kreutzer, M. T., Kapteijn, F., Moulijn, J. A., Kleijn, C. R. & Heiszwolf, J. J., 2005, Inertial and interfacial effects on pressure drop of Taylor flow in capillaries, *AIChE J.*, 51(9), 2428-2440.

Moriyama, K. & Inoue, A., 1996, Thickness of the liquid film formed by a growing bubble in a narrow gap between two horizontal plates, *J. Heat Transfer, Trans. ASME*, 118, 132-139.

Takamasa, T. & Kobayashi, K., 2000, Measuring interfacial waves on film flowing down tube inner wall using laser focus displacement meter, *J. Multiphase Flow*, 26(9), 1493-1507.

Taylor, G. I., 1961, Deposition of a viscous fluid on the wall of a tube, *J. Fluid Mech.*, 10(2), 161-165.

Thome, J. R., Dupont, V. & Jacobi, A. M., 2004, Heat transfer model for evaporation in microchannels. Part I: presentation of the model, *Int. J. Heat Mass Transfer*, 47(14-16), 3375-3385.

Utaka, Y., Okuda, S. & Tasaki, Y., 2007, Structure of micro-layer and characteristics of boiling heat transfer in narrow gap mini-channel system, *Trans. of the JSME, Series B*, 73(733), 1929-1935.